ELSEVIER

Chemical Engineering Journal 73 (1999) 217–227

Chemical Engineering Journal

Pressure drop modelling for liquid feed direct methanol fuel cells Part 1. Model development

P. Argyropoulos*, K. Scott, W.M. Taama

Chemical and Process Engineering Department, University of Newcastle upon Tyne, Merz Court, Newcastle upon Tyne NE1 7RU, UK

Received 17 August 1998; received in revised form 9 February 1999; accepted 14 February 1999

Abstract

A pressure drop model is presented for the direct methanol fuel cell, based on the homogeneous two-phase flow theory and mass conservation equation, which describes the hydraulic behaviour of an experimental large cell (active area 272 cm^2). The model allows an assessment of the effect of operating parameters, e.g. temperature gradient, current density, flow rate and pressure on pressure losses in the anode and the cathode side of the cell. It is designed to assist the fuel cell system designer to estimate flow and pumping requirements, tube sizing and auxiliary equipment and to be used to calculate flow distribution through fuel cell stack manifolds.

Keywords: Direct methanol fuel cell; Pressure drop modelling; Stacks; Two-phase flow

1. Introduction

Direct methanol fuel cells (DMFC), using a solid polymer electrolyte (SPE) membranes, e.g. Nafion® are considered as highly promising power sources, especially for vehicular applications. In principle this type of fuel cells has many important attributes; quick refuelling, low temperature and pressure operation, low market price of methanol, the use of the existing fuel distribution infrastructure, no liquid electrolyte and compact cell design. The main drawbacks of the cell to date are; methanol crossover through the membrane, with the production of a mixed potential at the cathode and a loss of fuel efficiency, and the lack of a highly active, cheap and efficient electrocatalyst [1,2].

A variety of research groups have been active in the research of direct methanol fuel cells and this has led to improved overall cell design and the production of significant power output of some 300 mW cm^{-2} [3–13]. Most of the work on fuel cells has focused on small cells, of active area less than 40–50 cm^2. As the DMFC system was not fully developed it was easier to use small cells of extremely simple design, to minimise costs and minimise difficulties in system engineering on scaling up. As soon as power performance reached a critical level a demand was created from industry for scaling up the cells and building fuel cell stacks capable of delivering electrical power of the order of kilowatts.

On scale up, thermal management and flow distribution become important issues that should be solved before building a successful DMFC stack. Flow distribution is critical, since, if both fluids are not distributed evenly, there can be localised feed or oxidant starvation, which will lower the cell performance. In addition this could lead to localised carbon dioxide accumulation which again can cause instabilities in both short- and long-term operation. The present model deals with the problem of pressure losses and flow distribution inside large scale DMFCs, (272 cm^2 active area, 0.5 kW nominal power output) under development at Newcastle. A schematic representation of the stack is presented in Fig. 1.

2. Anode side flow bed modelling

The model developed here is based on a flow bed design, developed by our group, which is presented in Fig. 2. It consists of a main flow bed, of 57 parallel channels, and two triangular inlet/outlet sections, of a spot flow bed design, which help to achieve a uniform flow distribution and efficient gas removal. The model for the anode side is based on the following assumptions:

*Coresponding author.

1385-8947/99/$ – see front matter
PII: S1385-8947(99)00038-8

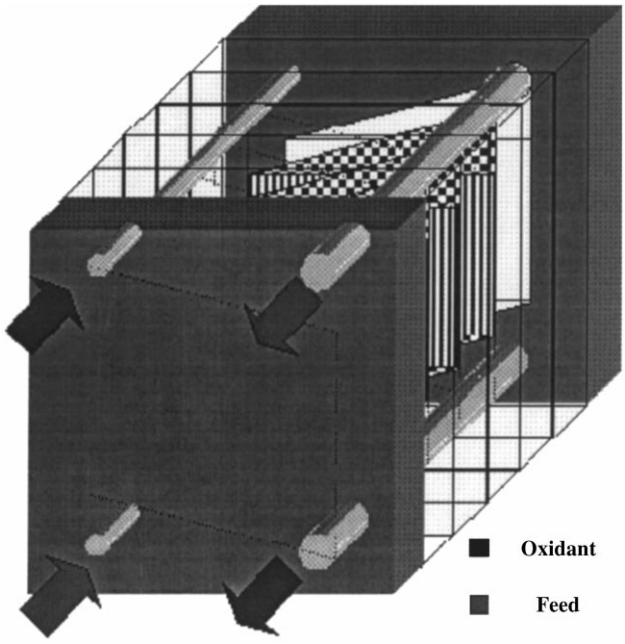

Fig. 1. An internally manifolded fuel cell stack.

- The current is assumed to be uniformly distributed. Polarisation characteristics are largely controlled by the anode side of the DMFC, which is a liquid feed system. The conversion of methanol in the cell is low and in addition, methanol oxidation is half order in methanol concentration. Thus current distribution is not a problem to the DMFC.
- The temperature of the two-phase flow rises linearly, from the inlet to the outlet, as a function of the active area.
- The temperature gradient between the inlet and the outlet of the plate is relatively small and hence the physical properties of the pure reactants and products are assumed constant.
- The physical properties of the two-phase mixture are a function of the reactants/products mass fractions.
- No methanol exists in the gas phase, i.e. the vaporisation of methanol into carbon dioxide is small. This assumption is adopted for convenience of solution. A model is currently being developed which determines the extent of vaporisation of methanol, and water, as a function of operating parameters and will be incorporated into this pressure drop model when it has been evaluated.
- Temperature is below the water boiling point so that all water remains in the liquid phase
- Reactants/products are consumed/formed as calculated according to Faraday's law.
- The hydraulic resistance of the spots in the two triangular sections is considered as negligible.

The pressure drops in the triangular spot sections are considered to be those associated with gradual enlarging and contracting ducts. Additional friction loss due to the spots can be accommodated, in the first instance, by using an equivalent diameter approach. The pressure drops in the inlet and outlet manifolds may cause a significant resistance to the flow especially in the case of the anode side of the cell.

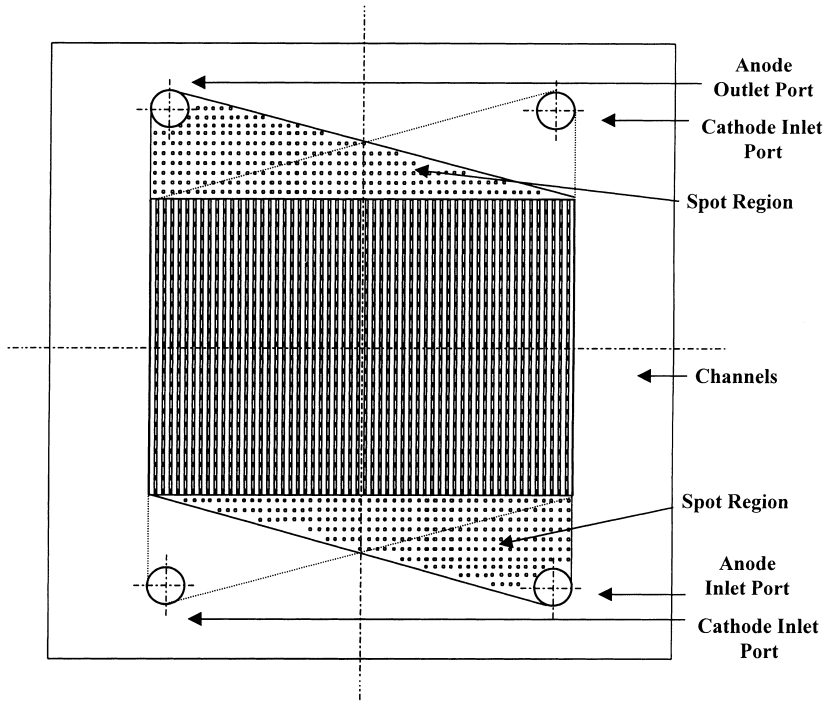

Fig. 2. Newcastle developed flow bed design.

Incorporating a relevant model for this would detract from the aim of model, which is to assess the hydraulic behaviour of the potential flow bed design and not an actual stack system. However, both of the above factors will be incorporated to a later model development.

During liquid feed DMFC operation, the aqueous methanol solution is fed, through a number of slots in the periphery of the manifold, to the anode side of each cell in the stack. Since the stack is operated at temperatures below 100°C, we can assume that the liquid feed remains liquid at the moment it enters the cell through the slot, and hence no vapour or carbon dioxide gas exists. Thus, for the cell i at the point of entrance we have the following mass flow rates:

$$\dot{m}_{\mathrm{H_2O,in}} = \dot{Q}_i \times \rho_{\mathrm{H_2O}} \left[1 - \left(\frac{\dot{Q}_i \times C_{\mathrm{MeOH}} \times \mathrm{MW}_{\mathrm{MeOH}}}{\rho_{\mathrm{MeOH}}} \right) \right] \tag{1}$$

$$\dot{m}_{\mathrm{MeOH,in}} = (\dot{Q}_i \times C_{\mathrm{MeOH}} \times \mathrm{MW}_{\mathrm{MeOH}}) \tag{2}$$

where $\dot{Q}_i$ is the solution flow rate entering cell i, C_{MeOH} is the methanol concentration (mol dm^{-3}) in the aqueous methanol feed solution, MW is the molecular mass of each reactant/product and ρ is the density.

The reactions that occur in the direct methanol fuel cell are Anode side:

$$\mathrm{CH_3OH + H_2O \rightarrow 6e^- + 6H^+ + CO_2}, \tag{3}$$

and at the cathode:

$$\tfrac{3}{2}\mathrm{O_2 + 6e^- + 6H^+ \rightarrow 3H_2O} \tag{4}$$

which can be combined and give the overall reaction:

$$\mathrm{CH_3OH + \tfrac{3}{2}O_2 \rightarrow 2H_2O + CO_2} \tag{5}$$

At the outlet of the anode flow bed plate the inlet volume of aqueous methanol solution is reduced by the amount of methanol consumed by electrochemical reaction plus the methanol transferred across the membrane by electro-osmosis, i.e. methanol crossover:

$$\dot{m}_{\mathrm{MeOH,out}} = \left(\dot{Q}_i \times C_{\mathrm{MeOH}} \times \mathrm{MW}_{\mathrm{MeOH}}\right) - \frac{S_{\mathrm{MeOH}} \times j \times A_{\mathrm{active}} \times \mathrm{MW}_{\mathrm{MeOH}}}{100 \times ne \times F} - \frac{x_{\mathrm{drag,MeOH}} \times j \times A_{\mathrm{active}} \times \mathrm{MW}_{\mathrm{MeOH}}}{1000 \times n \times F} \tag{6}$$

The electrochemical reaction also consumes water (one mole of methanol per mole of water) which is in the methanol aqueous solution. The electro-osmotic drag of water across the membrane, i.e. the number of water molecules that are dragged with each H^+ ion, depends on the membrane material and temperature [14–22]. Values vary between 2 and 5 molecules per H^+ and hence an average value of 2.5 will be used in the model development. Hence the total quantity of water removed from the anode stream is:

$$\dot{m}_{\mathrm{H_2O,out}} = \dot{Q}_i \rho_{\mathrm{H_2O}} \left(1 - \left(\frac{\dot{Q}_i \times C_{\mathrm{MeOH}} \times \mathrm{MW}_{\mathrm{MeOH}}}{\rho_{\mathrm{MeOH}}} \right) \right) - \frac{S_{\mathrm{H_2O}} \times j \times A_{\mathrm{mea}} \times \mathrm{MW}_{\mathrm{H_2O}}}{100 \times ne \times F} - \frac{x_{\mathrm{drag,H_2O}} \times j \times A_{\mathrm{mea}} \times \mathrm{MW}_{\mathrm{H_2O}}}{1000 \times n \times F} \tag{7}$$

Finally the amount of carbon dioxide gas produced is a direct function of the current density:

$$\dot{m}_{\mathrm{CO_2,out}} = \frac{A_{\mathrm{active}} \times \mathrm{MW}_{\mathrm{CO_2}} \times j \times S_{\mathrm{CO_2}}}{100 \times ne \times F} \tag{8}$$

It would be more useful for modelling to have a general expression, which gives the mass fraction of each element as a function of increasing flow bed length. For this purpose the active area is divided into three sections (see Fig. 3): (1) the triangular shaped inlet section, (2) the main body of the flow bed with the parallel channels, and (3) the triangular outlet section.

2.1. Anode triangular inlet section

In order to model the first section we use an expression that correlates the active area with increasing flow bed length:

$$A_{\mathrm{active,I}}(y) = \frac{y^2 \times w_{\mathrm{fb}}}{2 \times l_{\mathrm{I}}} \tag{9}$$

In the gradually enlarging triangular section the hydraulic diameter is equal to

$$d_{\mathrm{H,ge}}(y) = \frac{4 \times \text{void volume}}{\text{wetted area}} = \frac{2 \times y \times w_{\mathrm{fb}} \times c_{\mathrm{d}}}{[(l \times c_{\mathrm{d}}) + (y \times w_{\mathrm{fb}})]} \tag{10}$$

where l_{I} is the length of the triangular entry section and w_{fb} is the maximum width of the bed.

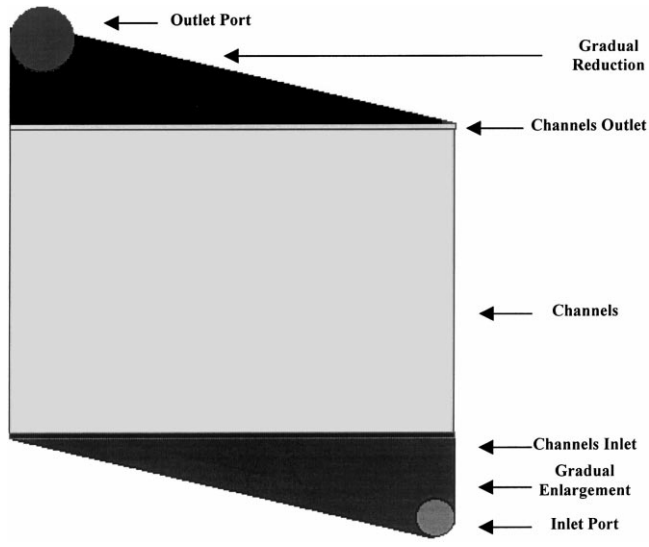

Fig. 3. Schematic representation of the various anode flow bed subdivisions.

In the view of many other uncertainties in two phase flow correlations, the friction factors are adequately represented as [23]:

$$f = \begin{cases} \dfrac{64}{\mathrm{Re}} & \text{for Re} < 2000 \quad \text{(Poiseuille equation)} \\ \dfrac{0.32}{\mathrm{Re}^{0.25}} & \text{for Re} > 2000 \quad \text{(Blasius equation)} \end{cases} \tag{11}$$

As the aqueous methanol solution enters the flow bed it undergoes a gradual enlargement from the initial inlet slot length to the final active area width. The pressure drop can be calculated, as a first approximation, by ignoring the existence of spots in that area, using of the well known formula for the resistance of a gradually enlarging duct:

$$K = K'\left[1 - \left(\frac{d}{D}\right)^2\right]^2 \tag{12}$$

where K' is a constant with values given in Table 1. L is the length of the triangular area. Theoretically, d and D are the initial and the final diameter of the duct, but in our case we will use the initial and final width of the duct defined within the model step length.

Finally the pressure drop for the flow through that area can be calculated [24] from

$$\Delta P = \int_0^{l_1} \left[G^2(y) \left\{ \frac{2(yf(y) + K_I)\upsilon_f(y)}{d_{H,ge}} \times \left(1 + \frac{x_0(y)\upsilon_{fg}(y)}{2\upsilon_f(y)}\right) + (\upsilon_f(y) - \upsilon_{fi}(y)) + \upsilon_{fg}(y)x_0(y) \right\} + \frac{gy}{\upsilon_{fg}(y)x_0(y)} \ln\left(1 + x_0(y)\frac{\upsilon_{fg}(y)}{\upsilon_f(y)}\right) \right] \mathrm{d}y \tag{13}$$

The first term of Eq. (13) denotes the frictional pressure drop for single phase and two-phase conditions, respectively. The second term accounts for the acceleration of the liquid due to a change in the specific volume, which produces a small pressure drop. The third term represents acceleration pressure drop for the two-phase flow. The fourth and the fifth terms of Eq. (13) denote the single phase and two-phase gravitational head, respectively. In the aforementioned formula υ_{fg} is the difference in specific volumes between the gas and the liquid phase, υ_{fi} is the liquid specific volume at the inlet temperature, υ_f is the liquid phase specific volume, and υ_g is the gas phase specific volume. All the quantities that refer to two component mixtures will be calculated as weighted averages based on the mixture mass fractions.

Table 1
Values of K′

((D−d)/2L])	0.05	0.10	0.20	0.30	0.40	0.50	0.80
K′	0.14	0.20	0.47	0.76	0.95	1.05	1.10

Obtaining a general analytical expression for the integral of Eq. (13) that gives the pressure drop is quite difficult. Thus numerical integration is preferred using the trapezoidal rule.

$$\Delta P = \sum_{i=0}^{i=400} \left(\frac{\Delta y}{2} \times (\Delta P[i] + \Delta P[i-1]) \right) \tag{14}$$

In order to increase accuracy a large number of steps are used ($\Delta y = 10^{-4}$ m).

2.2. Anode parallel channel flow bed

For modelling the second region that is formed from 57 identical parallel channels, an expression that correlates the active area with the channel cross section area is needed. This will be a correction factor magnifying the real channel cross-section area for those quantities, which are electrochemically dependable. In our case, and in accordance with the assumptions stated above, we have:

$$\delta = \frac{w_{\text{flow bed}}}{N} \tag{15}$$

Hence the active area is calculated as

$$A_{\text{active,II}}(y) = (\delta \times c_w) \times y \tag{16}$$

The total flow bed resistance will be equal to the number of channels multiplied by the individual channel flow resistance. All these are valid under the assumption that flow is equally distributed to all channels. An extensive flow visualisation study [25,26] showed this, and hence such an assumption can be used for modelling. Fig. 4 presents a frame of the liquid flow developing in the anode chamber of a DMFC, captured with the aid of a high-speed camera, which supports the aforementioned assumption.

To increase model accuracy two further hydraulic resistances have to be added. These refer to the sharp edged inlet and outlet of each channel. The first one is the hydraulic resistance that the fluid experiences as it leaves the triangular inlet section and enters the channels. According to the literature this can be calculated as

$$K = 0.5 \tag{17}$$

The second resistance accounts for the fact that flow from each channel is suddenly discharged from the narrow channels to the small open space between the channel outlets and the spot area. This resistance can be calculated as:

$$K = 1.10 \tag{18}$$

The hydraulic diameter for that region is defined as

$$d_{H,II} = \frac{2 \times c_w \times c_d}{(c_w + c_d)} \tag{19}$$

where c_d is the depth of the flow bed, c_w is the channel width.

Finally, the total pressure drop through that section is calculated from the same Eq. (13). According to the model

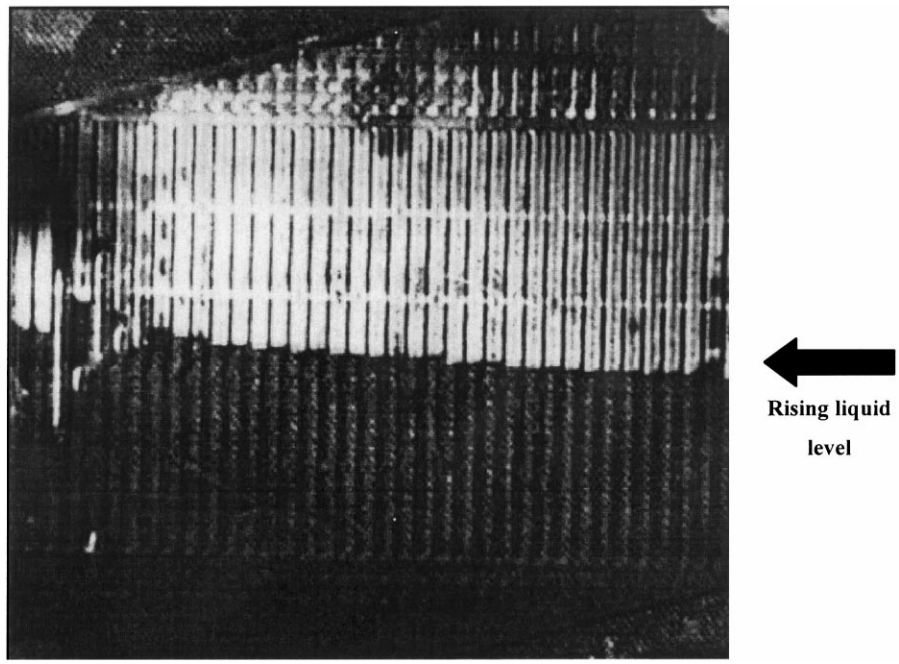

Fig. 4. Frame captured with the aid of a high-speed camera and shows the uniformly distributed flow in the parallel channels main flow bed.

assumptions the pressure drop reduces to

$$\Delta P = \sum_{i=0}^{i=1200} \left(\frac{\Delta y}{2} \times (\Delta P[i] + \Delta P[i-1]) \right) \tag{20}$$

2.3. Anode triangular outlet section

In order to model the third triangular section we need an expression that correlates the active area with increasing flow bed length:

$$A_{\text{active,III}}(y) = \left[\left(\frac{w_{\text{fb}} \times l_{\text{III}}}{2} \right) - \left(\frac{(l_{\text{III}} - y) \times w_{\text{fb}} (1 - (y/l_{\text{III}}))}{2} \right) \right] = \left[\frac{w_{\text{fb}}}{2 \times l_{\text{III}}} (2 y l_{\text{III}} - y^2) \right] \tag{21}$$

where l_{III} is the length of the triangular outlet section and w_{fb} is the maximum width of the flow bed. The hydraulic diameter for the case of the gradually decreasing triangular section is

$$d_{\text{H,gd}}(y) = \frac{4 \times \text{void volume}}{\text{wetted area}} = \frac{2 \times (l - y) \times w_{\text{fb}} \times c_{\text{d}}}{[(l \times c_{\text{d}}) + ((l - y) \times w_{\text{fb}})]} \tag{22}$$

The last hydraulic resistance to fluid flow on entering this section is due to the gradual decrease in the cross section. As a first approximation this can be calculated using the formula for the gradually reducing duct:

$$K = 0.05 \tag{23}$$

Again the total pressure drop through that section is calculated from the same Eq. (13). According to the model assumptions made previously the pressure drop reduces to

$$\Delta P = \sum_{i=0}^{i=400} \left(\frac{\Delta y}{2} \times (\Delta P[i] + \Delta P[i-1]) \right) \tag{24}$$

3. Cathode side flow bed modelling

In a practical DMFC stack air should be used as the oxidant. This means that either warm pre-humidified or dry compressed air is supplied to the cathode side. Of course supplying pure oxygen gas may result in an enhancement in performance but is not an economic option for the gas supply. As air passes through the cathode side flow bed it diffuses through the carbon cloth to the catalyst layer where oxygen is consumed. A small quantity of nitrogen transfers through the membrane to the anode side but in general it is negligible. Thus, all the nitrogen is assumed to leave the cell with the rest of the cathode side exhaust gases. The cathode reaction produces water, which is added to the water and methanol, transferred electro-osmotically from the anode. Methanol reacts with the cathode platinum electrocatalyst, producing a mixed potential, which reduces the cell performance. The degree of methanol conversion is unknown, but definitely some methanol remains unreacted and leaves the cell with the condensate and the exhaust gases. If the entire methanol due to crossover reacts at the cathode the amount of carbon dioxide which will be formed is small compared with the amount of air passing through the cathode. If the entire methanol quantity stays in the cathode in the form of an aqueous solution its effect on the total liquid mass fraction will be small due to the large water production and crossover. Thus, in the present model it was

chosen to perform the calculations based on the assumption that the methanol which has crossed over is not oxidised in the cathode side flow bed. We are currently developing a model for methanol crossover and its cathode reaction, which also includes the vaporisation of methanol into the cathode gases with water vaporisation [27]. A value of almost 60% is quoted from several researchers but yet this is heavily dependent on the membrane type, the electrode fabrication technique, and the operating conditions. In all cases the overall amount of methanol remains small in comparison with the amount of water (produced and electro-osmotically transferred) present in the cathode side and it will not affect significantly the pressure drop behaviour. Hence, in low air flow rates there is a strong possibility that the air stream will be fully saturated with water but it will never be saturated with methanol.

There are a number of important differences between the cathode and anode sides of the cell. The first is the different orientation of flow in that the cathode air is supplied from the top port of the plate and leaves from the bottom, hence the two fluids are flowing counter-currently. Except from enhancing heat transfer characteristics (if we treat the cell as a device in which heat transfer is from the hot anode stream to the cold cathode stream), this configuration reduces a practical problem created by the difficulty in removing liquid water from the cathode compartment. This can result in cathode flooding and hence to deterioration in performance [3]. Using the gravitational force alleviates this problem to some extent. The second significant difference in the two systems, is that the anode side contains a liquid–gas system while the cathode side is mainly a gas–liquid system. In practice water and methanol traces are present in the cathode as small droplets dispersed on the plate surface, as shown in the visualisation study conducted in our laboratory. This results in two possible operating conditions: either single-phase flow when the air inlet stream is not fully saturated with water, and methanol, at the local temperature and pressure conditions or a two-phase flow when the air stream is fully saturated. The transition of the two types of flow can occur at any position in the flow bed depending upon the prevailing operating conditions; temperature pressure and current density.

The present model compares the anode and cathode pressure drop performance with the same configuration and orientation. This is done so that the results are fully comparable and of general use. In the case of the downward flow configuration, described above, there is an improvement in the pressure drop characteristics of the cathode side. This feature will be assessed with the aid of the model in the second part of that paper.

Several assumptions are made in order to describe the cathode system:

- Air will always become humidified with water and the amount of water is calculated as a function of temperature, and pressure, of the cathode side.
- Air enters at room temperature and no prehumidification system is used.
- The current is assumed to be uniformly distributed.
- The temperature of the two-phase oxidant rises linearly from the inlet temperature to the outlet as a function of the active area.
- The physical properties of the two-phase mixture are a function of the reactants/products mass fractions
- Air acquires locally and instantaneously the available water and methanol until it becomes fully saturated at the local temperature and pressure conditions.
- Reactants/products are consumed and formed is accordance with Faraday's law.
- The hydraulic resistance of the spots in the two triangular sections is neglected.
- Physical properties are calculated as weighted averages of components mass fractions.

Before proceeding with the cathode side flow bed pressure modelling it is essential to present a simplified calculation methodology for estimating the water and methanol saturation content of the air at the local temperature and pressure conditions. The cell is assumed to contain liquid water over its cross section, and the water vapour pressure is assumed for simplicity to obey Dalton's and Raoult's laws:

$$p_{H_2O} = y_{H_2O,v} P_{cathode} = y_{H_2O,l} p^s_{H_2O} \tag{25}$$

where $y_{H_2O,v}$ is the mole fraction of water vapour in the cathode side flow bed, $y_{H_2O,l}$ is the liquid phase mole fraction which is a function of methanol concentration, and $p^s_{H_2O}$ the vapour pressure of pure water which is a function of temperature. The mole fraction of water is given by

$$y_{H_2O} = \frac{p^s_{H_2O}(T)}{P_{cathode}} \tag{26}$$

where $p^s_{H_2O}(T)$ in Pa, is calculated according to Wagner equation as

$$\ln\left(\frac{p^s_{H_2O}}{P_{c,H_2O}}\right) = \left[\left(\frac{1}{1-x_{H_2O}}\right) \times \left(-7.76451x_{H_2O} + 1.45838x^{1.5}_{H_2O} - 2.77580x^3_{H_2O} - 1.23303x^6_{H_2O}\right)\right] \tag{27}$$

where T_{c,H_2O} is water critical temperature (647.3 K) and P_{c,H_2O} water critical pressure (221.2 bar).

$$x_{H_2O} = \left(1 - \frac{T}{T_{c,H_2O}}\right) \tag{28}$$

The air is also saturated with methanol, which obeys Dalton's and Raoult's laws:

$$p_{MeOH} = y_{MeOH,v} P_{cathode} = y_{MeOH,l} p^s_{MeOH} \tag{29}$$

where $y_{MeOH,v}$ is the mole fraction of methanol vapour in the cathode side flow bed, $y_{MeOH,l}$ is the liquid phase mole

fraction which is only a function of the methanol concentration, and p^{s}_{MeOH} is the vapour pressure of pure methanol which is a function of temperature.

Methanol vapour pressure can be calculated again with the aid of the Wagner equation:

$$\ln\left(\frac{p^{s}_{MeOH}}{P_{c,MeOH}}\right) = \left[\left(\frac{1}{1-x_{MeOH}}\right) \times \left(-8.54796x_{MeOH} + 0.76982x^{1.5}_{MeOH} - 3.10850x^{3}_{MeOH} - 1.54481x^{6}_{MeOH}\right)\right] \quad (30)$$

where $T_{c,MeOH}$ is methanol critical temperature (512.6 K) and $P_{c,MeOH}$ water critical pressure (80.9 bar)

$$x_{MeOH} = \left(1 - \frac{T}{T_{c,MeOH}}\right) \quad (31)$$

3.1. Cathode triangular inlet section

At this point we calculate the amount of methanol and water that are needed to saturate the incoming airflow. We assume that saturation is instantaneous and that the airflow takes all the available methanol and water till it becomes fully saturated at the given local temperature and pressure conditions. The vapour pressure of methanol and water is calculated as indicated above, and hence the mole fractions of water and methanol vapour are known. All the quantities are functions of temperature and, indirectly, of increasing flow bed length.

The mass flow rates in each element of region (I), as a function of increasing flow bed length, are

$$\dot{m}(y)_{MeOH} = \frac{x_{drag,MeOH} \times j \times A_{active,I}(y) \times MW_{MeOH}}{1000 \times n \times F} \quad (32)$$

$$\dot{m}(y)_{H_2O} = \frac{S_{H_2O,p} \times A_{active,I}(y) \times MW_{H_2O}}{100 \times ne \times F} + \frac{x_{drag,H_2O} \times j \times A_{active,I}(y) \times MW_{H_2O}}{1000 \times n \times F} \quad (33)$$

$$\dot{m}(y)_{O_2} = \left(10^{-3} \times \frac{0.233 \times P_{cathode} \times \dot{Q} \times MW_{air}}{R \times T_{cathode,in}}\right) - \frac{S_{O_2} \times j \times A_{active,I}(y) \times MW_{O_2}}{1000 \times n \times F} \quad (34)$$

$$\dot{m}(y)_{N_2} = 10^{-3} \times \frac{0.767 \times P_{cathode} \times \dot{Q} \times MW_{air}}{R \times T_{cathode,in}} \quad (35)$$

$$\dot{m}(y)_{CO_2} = 0 \quad (36)$$

As the air enters the cathode flow bed it undergoes a gradual enlargement from the initial inlet slot length to the final active area width. This can be calculated, as a first approximation, and by ignoring the existence of spots in that area, with the use of the aforementioned formula (Section 2.1) for the resistance of a gradually enlarging duct.

Finally the pressure drop is calculated from

$$\Delta P = \int_0^{l_l} \begin{cases} \left[G^2(y)\left(\frac{2(yf(y)+K_1)\upsilon_g(y)}{d_{H,ge}} + (\upsilon_g(y) - \upsilon_{gi}(y))\right) + \frac{gy}{\upsilon_{fg}(y)}\right] dy \\ \left[G^2(y)\left\{\frac{2(yf(y)+K_1)\upsilon_g(y)}{d_{H,ge}}\left(1 + \frac{x_0(y)\upsilon_{fg}(y)}{2\upsilon_g(y)}\right) + (\upsilon_g(y) - \upsilon_{gi}(y)) + \upsilon_{fg}(y)x_0(y)\right\} + \frac{gy}{\upsilon_{fg}(y)x_0(y)}\ln\left(1 + x_0(y)\frac{\upsilon_{fg}(y)}{\upsilon_g(y)}\right)\right] dy \end{cases} \quad (37)$$

The first branch represents the pressure drop for single phase flow, i.e. when there is no liquid water or methanol in the flow bed, which is the case when the air stream is not fully saturated at the local temperature and pressure conditions. The first terms of the second branch denote the frictional pressure drop for single phase and two-phase flow conditions. The second term accounts for the acceleration of the gas due to a change in the specific volume, which produces a small pressure drop. The third term represents acceleration pressure drop for the two-phase flow. The fourth and the fifth terms of the equation denote the single phase and two-phase gravitational head, respectively. In the aforementioned formula, υ_{fi} is the difference in specific volumes between the gas and the liquid phase, υ_{fi} is the liquid specific volume at the inlet temperature, υ_f is the liquid phase specific volume and υ_g is the gas phase specific volume.

According to the model assumptions, the pressure drop reduces to

$$\Delta P = \sum_{i=0}^{i=400}\left(\frac{\Delta y}{2} \times (\Delta P[i] + \Delta P[i-1])\right) \quad (38)$$

3.2. Cathode parallel channel flow bed

The parameters that are used to calculate the pressure drop for the parallel channels, such as the hydraulic diameter, hydraulic resistances, etc., are the same as those for the anode side. Mass fractions, densities and the remaining physical properties are calculated as above for the inlet section. Finally the total pressure drop through the section is calculated using the same formula as above. Thus, the pressure drop for that section is

$$\Delta P = 57 \times \sum_{i=0}^{i=1200}\left(\frac{\Delta y}{2} \times (\Delta P[i] + \Delta P[i-1])\right) \quad (39)$$

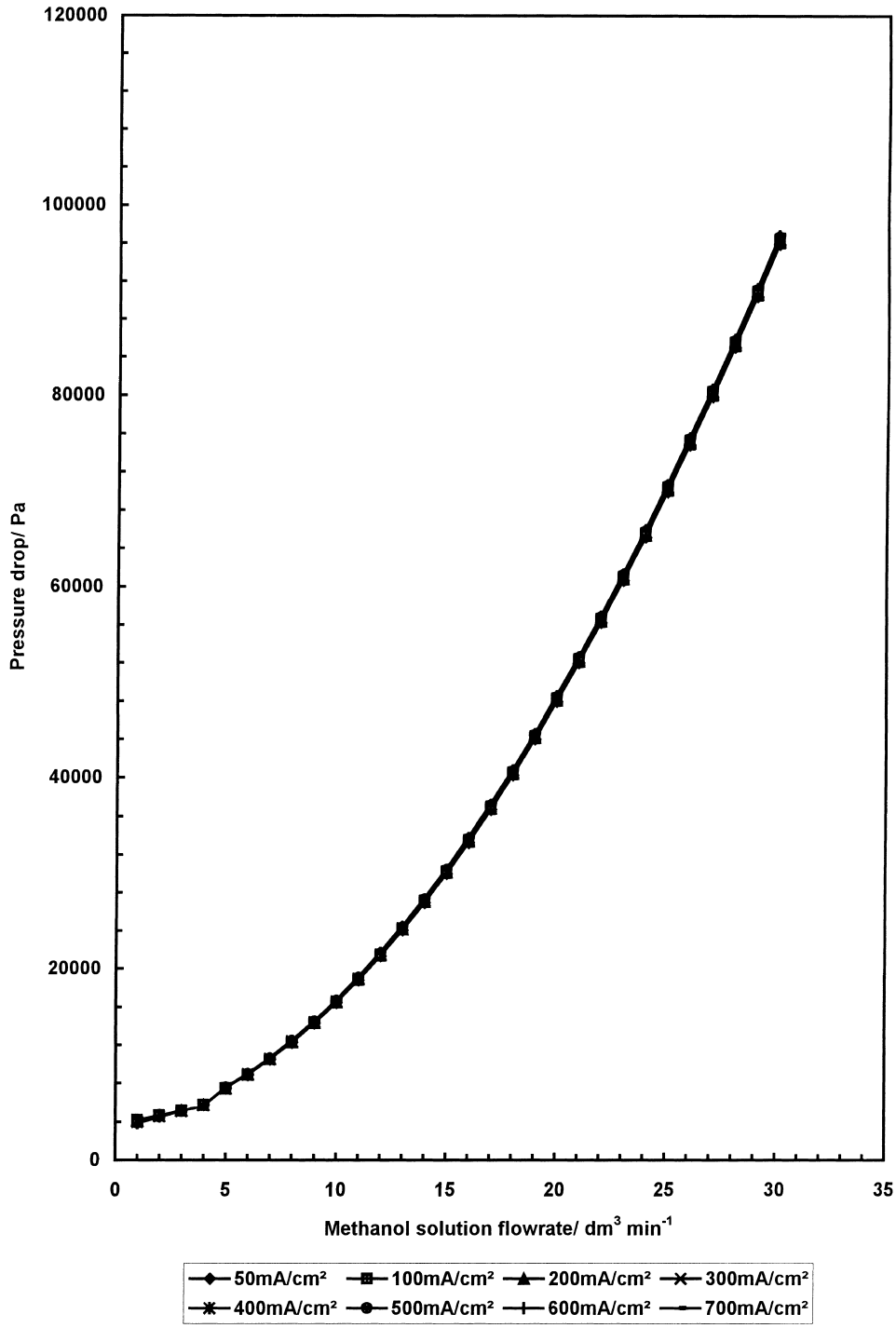

Fig. 5. Model predicted anode side pressure drop as a function of increasing methanol solution flowrate and operating current density.

3.3. Cathode triangular outlet section

The analysis for that section is exactly the same as for the preceding triangular inlet section. Active area as a function of increasing flow bed length, the hydraulic diameter, and the added hydraulic resistances utilise the same expressions as for the analysis of the anode side triangular outlet section.

4. Calculation procedure

Obtaining an analytical solution for both integrals, which determine the pressure drop in both channels, is not possible. Some of the linear functions, used to describe physical quantities such as mass fractions, or liquid phase flow rate are equal to zero at the inlet of the flow bed. In addition, at the cathode side there will be a change from single-phase to

two-phase flow at some location in the channel. This change depends on a variety of system operating parameters: current density, air flow rate, degree of methanol, and water, crossover, and the extent of external humidification (if used). This kind of system behaviour results in, locally, values of some derived quantities equal to infinity, which upsets the calculation procedure. This problem is solved with control loops, which check continuously the system flow conditions and divert the calculation routine to either single or two-phase conditions for the cathode side. The problem in the anode side is less severe, and is solved with the aid of a set of proper initial values.

The inputs to the model are feed and oxidant flow rates, inlet and outlet temperatures, operation pressure, and methanol solution concentration. As outputs, the model returns local Reynolds numbers, local, sectional and total pressure drop, pressure drop components, and with the aid of an extra routine it calculates outlet gas, liquid and total flow rates, and the solution concentration leaving the anode side.

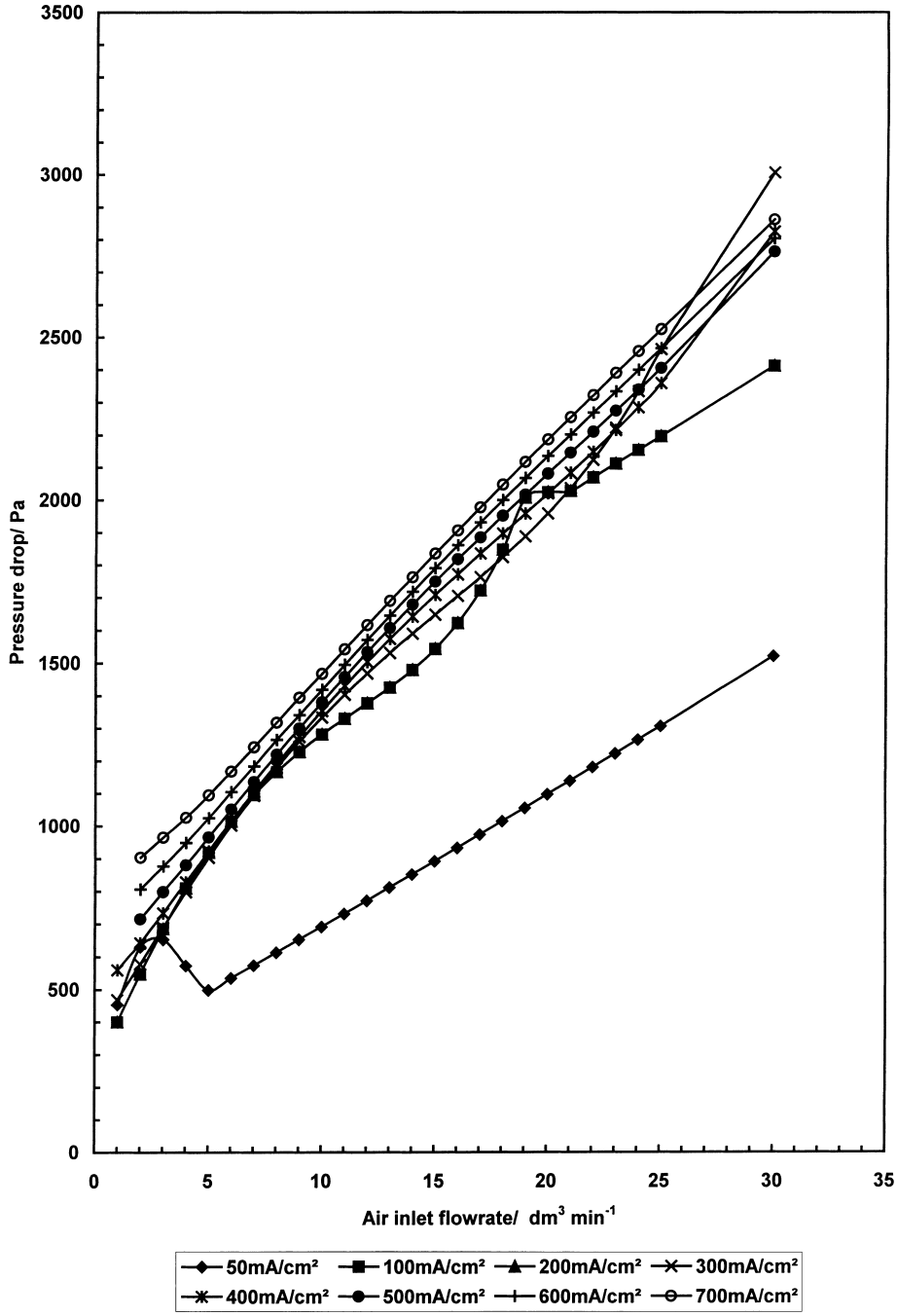

Fig. 6. Model predicted cathode side pressure drop as a function of increasing air flowrate and operating current density.

Typical predicted pressure drop profiles for the anode and cathode side of the DMFC as a function of increasing inlet flow rate and for different operating current densities are presented in Figs. 5 and 6. Fig. 5 shows predicted pressure drop profiles for increasing liquid phase inlet flow rate and for a range of operating current densities. In the lower and medium range flow rates (typically below 3.0 l/mm) the presence of carbon dioxide gas affects the hydraulic behaviour of the structure. More specifically the lift produced by the rising bubbles slightly reduces the pressure drop. As the flow rate increases, this effect tends to be less significant and the pressure drop is mainly due to the liquid phase friction losses, and increases quickly with increasing flow rate.

Fig. 6 presents equivalent pressure drop results for the cathode side. As expected the pressure drop in that side is comparatively low since it is contains almost pure gaseous flow. The anomalies in the predicted profiles are explained from the transition from two-phase flow to a single-phase flow, due to liquid phase depletion (gaseous phase is not fully saturated in water and methanol). With large airflow the pressure losses are modest (less than 0.3 bar) and hence the hydraulic behaviour of the cathode side is less of a problem, than the anode, in a large DMFC stack system.

Part II of this paper presents detailed results of the model simulation in which the effect of a range of operating parameters and variable are examined, and the associated mechanisms are discussed in detail.

5. Conclusions

A model for predicting the pressure drops in both the anode side and cathode side of a single large scale DMFC is developed. Based on the operation conditions of the system such as inlet stream volumetric flow rates, inlet stream temperatures, and operating pressures the model calculates the local mass balances, local Reynolds numbers and can predict the local and the overall pressure drops. The data are valuable for a DMFC system designer since they provide the means to asses the effect of altering system operating conditions on each cell compartment pressure drop. This can help avoid problems such as cathode side water flooding, due to insufficient water removal, membrane drying from excess water removal, and anode side gas management problems from insufficient carbon dioxide removal.

Acknowledgements

The authors would like to acknowledge The European Commission for supporting Mr P. Argyropoulos under a B20 TMR Marie Curie research training grant and the EPSRC for supporting Dr. W.M. Taama.

Appendix

Nomenclature

Symbols

A	area (m^2)
C	concentration ($mol/10^{-3}\ m^3$)
c_p	specific heat (J/kg K)
d_H	hydraulic diameter (m)
F	friction factor
F	faraday constant (A s/mol)
G	mass velocity ($kg/m^2\ s$)
G	standard gravitational acceleration (m/s^2)
H	convective heat transfer (W/m^2K)
J	current Density (mA/cm^2)
K	hydraulic resistance
L	length (m)
MW	molecular weight (10^{-3} kg/mol)
$\dot{m}$	mass flow rate (kg/s)
n	number of electrons transferred through the cell
N	number of channels
p	vapour pressure
P	pressure
Q	heat (W)
$\dot{Q}$	volumetric flowrate (m^3/s)
Re	Reynolds number
S	stoichiometric coefficient
T	temperature (K)
X_0	mass fraction of the dispersed phase

Subscripts

d	depth
f	liquid
fb	flow bed
fg	liquid–gas
g	gas
gf	gas–liquid
mea	membrane electrode assembly
w	width

Greek Letters

ΔH	reaction enthalpy (J/kg mol)
χ	electro-osmotic drag coefficient
δ	magnification coefficient
η	overpotential (V)
μ	viscosity (kg/m s)
ρ	density (kg/s)
υ	specific volume (kg/m^3)

References

[1] X. Ren, M.S. Wilson, S. Gottesfeld, High performance direct methanol polymer electrolyte fuel cells, J. Electrochem. Soc. 143(1) (1996) L12–L15.

[2] V.M. Schmidt, P. Brockerhoff, B. Hohlein, R. Menzer, U. Stimming, Utilization of methanol for polymer electrolyte fuel cells in mobile system, J. Power Sources 49 (1994) 299–313.
[3] T.I. Valdez, S.R. Narayanan, H. Frank, W. Chun, Direct methanol fuel cell for portable applications, in: Proc. Annual Battery Conf. on Applications and Advances, 1997, Long Beach, USA.
[4] A.K. Shukla, P.A. Christensen, A.J. Dickinson, A. Hamnett, A liquid feed solid polymer electrolyte direct methanol fuel cell, J. Power Sources 76(1) (1998) 54–59.
[5] A.K. Shukla, P.A. Christensen, A. Hamnett, M.P. Hogarth, A vapour-feed direct-methanol fuel cell with proton exchange membrane electrolyte, J. Power Sources 55 (1995) 87–91.
[6] S.R. Narayanan, G. Halpert, W. Chun, B. Jeffries-Nakamura, T.I. Valdez, H. Frank, S. Surampudi, The status of direct methanol fuel cell technology at JPL, in: 37th Power Sources Conf., 1996, Cherry Hill, NJ, USA.
[7] S.R. Narayanan, G. Halpert, W. Chun, B. Jeffries-Nakamura, T.I. Valdez, H. Frank, S. Surampudi, Recent advances in the performance of direct methanol fuel cells, in: Electrochemical Society Annual Meeting, 1996, Los Angeles, CA, USA.
[8] S.R. Narayanan, T. Valdez, N. Rohatgi, W. Chun, G. Halpert, Design of direct methanol fuel cell systems, in: 1998 Fuel Cell Seminar, 1998. Palm Springs, CA, USA.
[9] M. Hogarth, P. Christensen, A. Hamnett, A.K. Shukla, The design and construction of high performance direct methanol fuel cells 2. Vapour feed systems, J. Power Sources 69 (1997) 125–136.
[10] M. Hogarth, P. Christensen, A. Hamnett, A.K. Shukla, The design and construction of high performance direct methanol fuel cells 1. Liquid feed systems, J. Power Sources 69 (1997) 113–124.
[11] M.P. Hogarth, J. Munk, A.K. Shukla, A. Hamnett, Performance of a carbon-cloth bound porous carbon electrodes containing an electro-deposited platinum catalyst towards the electro-oxidation of the methanol in sulphuric acid electrolyte, J. Appl. Electrochem. 24 (1994) 85–88.
[12] K. Scott, W.M. Taama, J. Cruickshank, Performance of a direct methanol fuel cell, J. Appl. Electrochem. 28(3) (1998) 289–297.
[13] K. Scott, W.M. Taama, P. Argyropoulos, Engineering aspects of the direct methanol fuel cell system, J. Power Sources, 1999 in press.
[14] T.A.J. Zawodzinski, T.E. Springer, J. Davey, J. Valerio, J. Gottesfeld, Water transport properties of fuel cell ionomers, in: R.E.V. White, M.W. Stockel (Eds.), Modelling of Batteries and Fuel Cells, The Electrochemical Society, Pennigton, 1991, pp. 187–196.
[15] T.A. Zawodzinski, J. Derouin, J. Valerio, S. Gottesfeld, The water content dependence of electro-osmotic drag in proton-conducting polymer electrolytes, Electrochim. Acta 40(3) (1995) 297–302.
[16] T.A.J. Zawodzinski, T.E. Springer, J. Davey, R. Jestel, C. Lopez, J. Valerio, S. Gottesfeld, A comparative study of water uptake by and transport through ionomeric fuel cell membranes, J. Electrochem. Soc. 140(7) (1993) 1981–1985.
[17] T.A.J. Zawodzinski, C. Derouin, S. Radzinski, R.J. Sherman, V.T. Smith, T.E. Springer, S. Gottesfeld, Water uptake by and transport through Nafion 117 membranes, J. Electrochem. Soc. 140(4) (1993) 1041–1047.
[18] T.A. Zawodzinski, S. Gottesfeld, S. Shoichet, T.J. McCarthy, The contact angle between water and the surface of perfluorosulphonic acid membranes, J. Appl. Electrochem. 23 (1992) 86–88.
[19] D. Weng, J.S. Wainright, U. Landau, R.F. Savinell, Electro-osmotic drag coefficient of water and methanol in polymer electrolytes at elevated temperatures, J. Electrochem. Soc. 143(4) (1996) 1260–1263.
[20] J.T. Wang, R.F. Savinell, Simulation studies on the fuel cell electrode of a H2-02 polymer electrolyte fuel cell, Electrochim. Acta 3(15) (1992) 2737–2745.
[21] M.K. Ravikumar, A.K. Shukla, Effect of methanol crossover in a liquid feed polymer electrolyte direct methanol fuel cell, J. Electrochem. Soc. 143(8) (1996) 2601–2606.
[22] M.K. Ravikumar, Studies on direct methanol fuel cells and nickel–iron batteries, Indian Institute of Science, 1996.
[23] S.M. Walas, Chemical Process Equipment: Selection and Design, Butterworth-Heinemann Series in Chemical Engineering, H. Brenner (Ed.), Butterworth-Heinemann, Boston, USA, 1990.
[24] A.B. Datta, A.K. Majumdar, A calculation procedure for two phase flow distribution in manifolds with and without heat transfer, Int. J. Heat and Mass Transfer 26(9) (1983) 1321–1328.
[25] P. Argyropoulos, K. Scott, W.M. Taama, Gas evolution and power performance in direct methanol fuel cells, J. Appl. Electrochem. (1999) in press.
[26] P. Argyropoulos, K. Scott, W.M. Taama, Carbon dioxide evolution patterns in operating DMFC cells, Electrochim. Acta, 1998.
[27] K. Sundmacher, K. Scott, The impact of electrosmotic and pressure-driven mass transport on the limiting currents of a liquid-fed direct methanol polymer electrolyte fuel cell, Chem. Eng. Sci., 1999 in press.